

**Pedestrians in static crowds are not grains, but game players**

Thibault Bonnemain <sup>1,2,\*</sup> Matteo Butano <sup>3</sup> Théophile Bonnet<sup>4,3,†</sup> Iñaki Echeverría-Huarte <sup>5</sup> Antoine Seguin <sup>6</sup>  
 Alexandre Nicolas <sup>7</sup> Cécile Appert-Rolland <sup>4</sup> and Denis Ullmo <sup>3</sup>

<sup>1</sup>*Department of Mathematics, Physics and Electrical Engineering, Northumbria University, Newcastle upon Tyne, NE1 8ST, United Kingdom*

<sup>2</sup>*Department of Mathematics, King's College, London KCL WC2R 2LS, United Kingdom*

<sup>3</sup>*Université Paris-Saclay, CNRS, LPTMS, 91405 Orsay, France*

<sup>4</sup>*Université Paris-Saclay, CNRS, IJCLab, 91405 Orsay, France*

<sup>5</sup>*Laboratorio de Medios Granulares, Departamento de Física y Matemática Aplicada, Univ. Navarra, 31080 Pamplona, Spain*

<sup>6</sup>*Université Paris-Saclay, CNRS, FAST, 91405 Orsay, France*

<sup>7</sup>*Institut Lumière Matière, CNRS & Université Claude Bernard Lyon 1, 69622 Villeurbanne, France*



(Received 13 September 2022; accepted 1 February 2023; published 28 February 2023)

The local navigation of pedestrians is assumed to involve no anticipation beyond the most imminent collisions, in most models. These typically fail to reproduce some key features experimentally evidenced in dense crowds crossed by an intruder, namely, transverse displacements toward regions of higher density due to the anticipation of the intruder's crossing. We introduce a minimal model based on mean-field games, emulating agents planning out a global strategy that minimizes their overall discomfort. By solving the problem in the permanent regime thanks to an elegant analogy with the nonlinear Schrödinger's equation, we are able to identify the two main variables governing the model's behavior and to exhaustively investigate its phase diagram. We find that, compared to some prominent microscopic approaches, the model is remarkably successful in replicating the experimental observations associated with the intruder experiment. In addition, the model can capture other daily-life situations such as partial metro boarding.

DOI: [10.1103/PhysRevE.107.024612](https://doi.org/10.1103/PhysRevE.107.024612)

**I. INTRODUCTION**

Although crowd disasters (such as the huge stampedes that grieved the Hajj in 1990, 2006, and 2015 [1]) are more eye-catching to the public, the dynamics of pedestrian crowds are also of great relevance in less dire circumstances. They are central when it comes to designing and dimensioning busy public facilities, from large transport hubs to entertainment venues, and optimizing the flows of people. Modeling pedestrian motion in these settings is a multiscale endeavor, which requires determining where people are heading (*strategic* level), what route they will take (*tactical* level), and, finally, how they will move along that route in response to interactions with other people (*operational* level) [2]. The *strategic* and *tactical* levels typically involve some planning to make a choice among a discrete or continuous set of options, such as targeted activities, destinations [2], paths (possibly knowing their expected level of congestion) [3], or, in the context of evacuations, egress alternatives [3,4]. These choices are often handled as processes of maximization (minimization) of a utility (cost), which may depend on lower-level information such as pedestrian density or streaming velocity [5,6].

The *operational* level deals with much shorter timescales and is generally believed to involve no planning ahead. Anticipatory effects are thus merely neglected in so-called *reactive* models, especially at high densities, possibly with the lingering idea that mechanical forces then prevail. For example, the popular social force model of Helbing and Molnar [7], still at the heart of several commercial software products, combines contact forces and pseudoforces (social forces) which, in the original implementation, are only functions of the agents' current positions (and possibly orientations). Some degree of anticipation has since been introduced into these models to better describe collision avoidance, e.g., by making the pseudoforces depend on future positions rather than current ones [8,9]. In a dual approach, the most imminent collisions can be avoided by scanning the whole velocity space [10–12] or a subset of it [13] in search of the optimal velocity. All these dynamic models, at best premised on a constant-velocity hypothesis, owe their high computational tractability to their relative shortsightedness. Note that, to mitigate these limitations, in particular, in the case of denser crowds, anticipated collisions beyond the most imminent one [14] or, at a more coarse-grained scale, local density inhomogeneities [5] can be taken into account.

In this paper, we argue that, even at the *operational* level, crowds in some daily-life circumstances display signs of anticipation that may elude the foregoing short-sighted models; this will be exemplified by the recently studied response of a dense static crowd when crossed by an intruder [15,16]. We purport to show that a minimal game theoretical approach,

\*Corresponding author: [thibault.bonnemain@kcl.ac.uk](mailto:thibault.bonnemain@kcl.ac.uk)

†Current address: Université Paris-Saclay, CEA, Service d'Etudes des Réacteurs et de Mathématiques Appliquées, 91191 Gif-sur-Yvette, France.

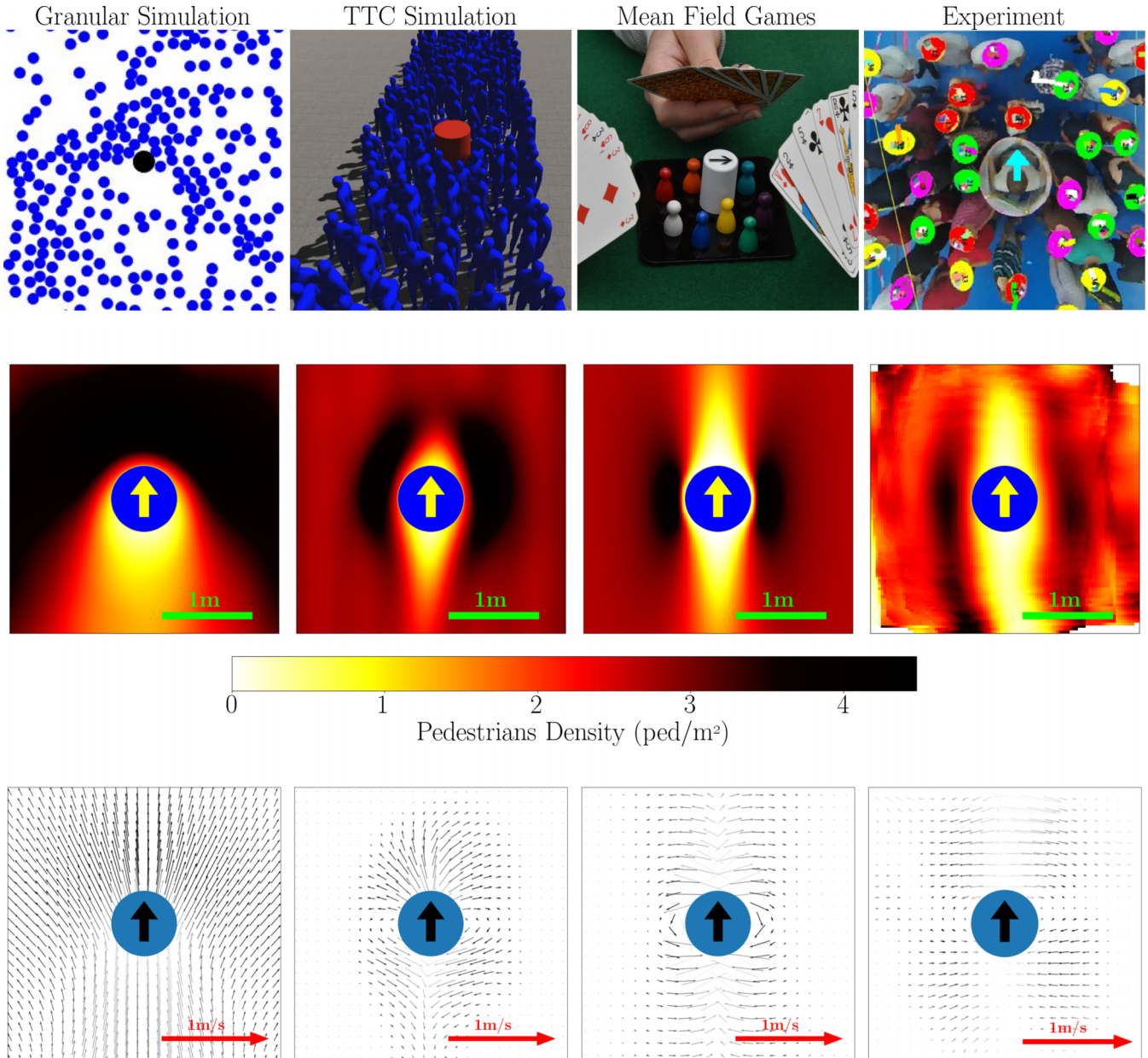


FIG. 1. Data (middle row) and velocity (bottom row) fields induced in a static crowd by a cylindrical intruder that crosses it; the transparency of the velocity arrows is linearly related to the local density. Column 1: Simulations of a monolayer of vibrated disks. Column 2: Simulations of an agent-based model wherein agents may anticipate the most imminent collision. All fields have been averaged over many realizations. Column 3: Results of the mean-field game introduced in this paper. Column 4: Controlled experiments of Ref. [15]. Note the relatively symmetrical density dip in front and behind the intruder, as well as the transverse moves. Columns 1–3: The crowd’s density and intruder’s size have been adjusted to match the experimental data (average density of 2.5 ped/m<sup>2</sup>). Details of simulations and videos showcasing time evolution can be found in the Appendix.

made tractable thanks to an elegant analogy between its mean-field formulation [17–19] and Schrödinger equation [20,21], can replicate the empirical observations for this example case, provided that it accounts for the anticipation of future costs. We use an experimental validation of mean field games (MFGs) as a relevant framework to study pedestrian dynamics. Beyond that particular example, the approach efficiently captures certain behaviors of crowds at the interface between the *operational* and *tactical* levels that are crucial to consider in attempts to improve the security of dense crowds.

## II. CROSSING A STATIC CROWD

Crossing a static crowd is a common experience in busy premises, from standing concerts and festivals to railway stations. Recently, small-scale controlled experiments [15,22] have shed light on trends that robustly emerged in the response of a crowd crossed by a cylindrical intruder, as displayed in Fig. 1 (right column). The induced response consists of a fairly symmetric density field around the intruder, displaying depleted zones both upstream and downstream from the

intruder, as well as higher-density regions on the sides. Consistently, the crowd's displacements are mostly transverse: pedestrians tend to simply step aside. A similar behavior—though more noisy—was observed when the intruder was a single pedestrian. Incidentally, a qualitatively similar response was filmed on a much larger scale in a dense crowd of protesters in Hong Kong, which split open to let an ambulance through [23].

As penetration by an intruder is a benchmark test for granular matter, it is instructive to compare the response of the two systems. Actually, the above crowd features strongly depart from the mechanical response observed in experiments [24,25] or simulations [26] of penetration into a granular monolayer below jamming, where grains are pushed forward by the intruder (see Fig. 1 (left column) and Movie S1 [27]) and accumulate downstream, instead of moving crosswise. More worryingly, these “mechanical” features are also observed (see Fig. 1 in Ref. [28]) in simulations of pedestrian dynamics performed with the social-force model [7], which rests on tangential and normal forces at contact and radial repulsive forces for longer-ranged interactions.

Introducing collision anticipation in the pedestrian model helps reproduce the opening of an agent-free tunnel ahead of the intruder, as illustrated with a time to (first) collision model (second column of Fig. 1 and Movie S2 [27]) directly inspired from Ref. [12], details of which can be found in Appendix B. However, even though the displacements need not align with the contact forces in this agent-based model, the displacement pattern diverges from the experimental observations, with streamwise (walk-away) moves that prevail over transverse (step-aside) ones. Indeed, such models rely on short-sighted agents who do not see past the most imminent collision expected from constant-velocity extrapolation.

Results will naturally vary with the specific collision-avoidance model and the selected parameters. Yet the failure of diverse state-of-the-art models to reproduce prominent experimental features suggests that an ingredient is missing in these approaches based on short-time (first-collision) anticipation.

### III. A GAME THEORETICAL APPROACH TO ACCOUNT FOR LOW-LEVEL PLANNING

To bring in the missing piece, we start by noticing that the observed behaviors are actually most intuitive: Pedestrians anticipate that it will cost them less effort to step aside and then resume their positions, even if it entails enduring high densities temporarily, than to endlessly run away from an intruder that will not deviate from its course. But accounting for this requires a change of paradigm compared to the foregoing approaches. Game theory is an adequate framework to handle conflicting impulses of interacting agents endowed with planning capacities: agents are now able to optimize their strategy taking into account the choices (or strategies) of others. So far, its use in pedestrian dynamics has mostly been restricted to evacuation tactics in discrete models [4,29,30]. Unfortunately, the problem becomes intractable when the number of interacting agents grows.

To overcome this quandary, we turn to MFG, introduced by Lasry and Lions [17,18] as well as Huang *et al.* [19]

in the wake of the mean-field approximations of statistical mechanics, and since used in a variety of fields, ranging from finance [31–33] to economics [34–36], epidemiology [37–39], sociology [37,40,41], and engineering [42–44]. While applications of MFG to crowd dynamics have already been proposed [3,40,45–48], our goal here is to demonstrate the practical relevance of this approach at the *operational* level, using an elementary MFG belonging to one of the models introduced by Lasry and Lions [17], and which can be thoroughly analyzed thanks to its connection with the nonlinear Schrödinger equation (NLS).

In the mean-field approximation, the  $N$ -player game is replaced by a generalized Nash equilibrium [49] where indistinguishable microscopic agents play against a macroscopic state of the system (a density field) formed by the infinitely many remaining agents. Consider a large set of pedestrians, the agents of our game, characterized by their spatial position (state variable)  $\mathbf{X}^i \equiv (x^i, y^i) \in \mathbb{R}^2$ , which we assume follows Langevin dynamics,

$$d\mathbf{X}_t^i = \mathbf{a}_t^i dt + \sigma d\mathbf{W}_t^i, \quad (1)$$

where the drift velocity (*control* variable)  $\mathbf{a}_t^i$  reflects the agent's strategy. In (1),  $\sigma$  is a constant and components of  $\mathbf{W}^i$  are independent white noises of variance one, accounting for unpredictable events. Agents are supposed identical, apart from their initial positions  $\mathbf{X}^i(t=0)$  and realizations of  $\mathbf{W}^i$ .

Each agent strives to adapt their velocity  $\mathbf{a}_t^i$  to minimize a cost functional we assume to take the simple form

$$c[\mathbf{a}^i](t, \mathbf{x}_t^i) = \left\langle \int_t^T \left[ \frac{\mu \mathbf{a}^2}{2} - (gm^e(t, \mathbf{x}) + U_0(\mathbf{x} - \mathbf{v}\tau)) \right] d\tau \right\rangle, \quad (2)$$

where  $\langle \cdot \rangle$  denotes averaging over all realizations of the noise for trajectories starting at  $\mathbf{x}_t^i$  at time  $t$ . In this expression, the term  $\mu \mathbf{a}^2/2$ , akin to a kinetic energy, represents the efforts required by the agent to enact their strategy (how much or how fast they have to move in this case), while the interactions with the other agents via the empirical density  $m^e(t, \mathbf{x}) = \sum_i \delta(\mathbf{x} - \mathbf{X}^i(t))/N$  are controlled by a parameter  $g < 0$ . Finally, the space occupied by the intruding cylinder, which moves at a velocity  $\mathbf{v} = (0, v)$ , is characterized by a potential  $U_0(\mathbf{x}) = V_0 \Theta(\|\mathbf{x}\| - R)$  that tends to  $V_0 \rightarrow -\infty$  inside the radius  $R$  of the cylinder and is zero elsewhere. Agents need to balance those three terms *over the whole duration  $T$  of the game*, which enables them to make costly but temporary moves if they lower the overall cost. For example, depending on the parameters, stepping aside into a high density region (a cost-inefficient strategy *a priori*) to let the intruder through may prove overall more efficient than running away from it; the first strategy implies paying a high cost upfront, but nothing afterward, while the second implies paying a comparatively low cost that, however, extends over the whole duration of the game, resulting in a potentially worse payoff.

In the presence of many agents, the density self-averages to  $m(t, \mathbf{x}) = \langle m^e(t, \mathbf{x}) \rangle_{\text{noise}}$  and the optimization problem (2) does not feature explicit coupling between agents anymore. It can then be solved by introducing the value function  $u(t, \mathbf{x}) = \min_{\mathbf{a}(\cdot)} c[\mathbf{a}](t, \mathbf{x})$ , which obeys a

Hamilton-Jacobi-Bellman (HJB) equation [18,50], with optimal control  $\mathbf{a}^*(t, \mathbf{x}) = -\nabla u(t, \mathbf{x})/\mu$ . Consistency imposes that  $m(t, \mathbf{x})$  is solution of the Fokker-Planck (FP) equation as-

$$\begin{aligned} \partial_t u(t, \mathbf{x}) &= \frac{1}{2\mu} [\nabla u(t, \mathbf{x})]^2 - \frac{\sigma^2}{2} \Delta u(t, \mathbf{x}) + gm(t, \mathbf{x}) + U_0(\mathbf{x} - \mathbf{v}t) \quad (\text{HJB}) \\ \partial_t m(t, \mathbf{x}) &= \frac{1}{\mu} \nabla \cdot [m(t, \mathbf{x}) \nabla u(t, \mathbf{x})] + \frac{\sigma^2}{2} \Delta m(t, \mathbf{x}). \quad (\text{FP}). \end{aligned} \quad (3)$$

The atypical forward-backward structure of Eqs. (3), highlighted by the opposite signs of Laplacian terms in the two equations, accounts for anticipation. The boundary conditions epitomize this structure: based on (2), the value function has terminal condition  $u(t = T, \mathbf{x}) = 0$ , while the density of agents evolves from a uniform initial distribution  $m(t = 0, \mathbf{x}) = m_0$ . In previous work, we evinced a formal but insightful mapping of these MFG equations onto a NLS [20,21,51], well studied in fields ranging from nonlinear optics [52,53] to Bose-Einstein condensation [54,55] and fluid dynamics [56,57].

We perform a change of variables  $(u(t, \mathbf{x}), m(t, \mathbf{x})) \mapsto (\Phi(t, \mathbf{x}), \Gamma(t, \mathbf{x}))$  through  $u(t, \mathbf{x}) = -\mu\sigma^2 \log \Phi(t, \mathbf{x})$ ,  $m(t, \mathbf{x}) = \Gamma(t, \mathbf{x})\Phi(t, \mathbf{x})$  [21]. The first relation is the usual Cole-Hopf transform [58]; the second corresponds to a Hermitization of Eqs. (3). In terms of the new variables  $(\Phi, \Gamma)$ , the MFG equations read

$$\begin{aligned} -\mu\sigma^2 \partial_t \Phi &= \frac{\mu\sigma^4}{2} \Delta \Phi + (U_0 + g\Gamma\Phi)\Phi \\ +\mu\sigma^2 \partial_t \Gamma &= \frac{\mu\sigma^4}{2} \Delta \Gamma + (U_0 + g\Gamma\Phi)\Gamma. \end{aligned} \quad (4)$$

Besides the missing imaginary factor associated with time derivation, these equations have exactly the structure of a NLS describing the evolution of a quantum state  $\Psi(t, \mathbf{x})$  of a Bose-Einstein condensate, with formal correspondence  $\Psi \rightarrow \Gamma$ ,  $\Psi^* \rightarrow \Phi$  and  $\rho \equiv |\Psi|^2 \rightarrow m \equiv \Phi\Gamma$ . This system, however, retains the forward-backward structure of MFG evidenced by mixed initial and final boundary conditions  $\Phi(T, \mathbf{x}) = 1$ ,  $\Gamma(0, \mathbf{x})\Phi(0, \mathbf{x}) = m_0(\mathbf{x})$ . Several methods have been developed to deal with NLS and most can be leveraged to tackle the MFG problem [21,59].

Self-consistent solutions of Eqs. (4) are obtained by iteration: (i) Assume  $m(t, \mathbf{x}) = m_{\text{in}}(t, \mathbf{x})$ ; (ii) solve the equation for  $\Phi$  backward in time with terminal condition  $\Phi(T, \mathbf{x}) = 1$ ; (iii) solve the equation for  $\Gamma$  forward in time with initial condition  $\Gamma(0, \mathbf{x}) = m_0(\mathbf{x})/\Phi(0, \mathbf{x})$ ; and (iv) iterate with  $\Phi(t, \mathbf{x})\Gamma(t, \mathbf{x}) = m_{\text{out}} \mapsto m_{\text{in}}$  until  $m_{\text{out}}$  is sufficiently close to  $m_{\text{in}}(t, \mathbf{x})$ . A video illustrating the evolution of the agents' density for a particular set of parameters, along with additional details about the numerical scheme, can be found in Appendix C.

Focusing on the *permanent* regime [60], for which we have experimental data [15], rather than on the transients associated with the intruder's entry or exit, further simplifies the resolution. In this regime, defined by time-independent density and velocity fields in the intruder's frame, the auxiliary

sociated with (1), given the drift velocity  $\mathbf{a}(t, \mathbf{x}) = \mathbf{a}^*(t, \mathbf{x})$ . As such, MFG can be reduced to a system of two coupled partial differential equations [17,18,20,21]:

functions  $\Phi$  and  $\Gamma$  are not constant in time, but they assume the trivial dynamics  $\Phi(t, \mathbf{x}) = \exp[\lambda t/\mu\sigma^2]\Phi_{\text{er}}(\mathbf{x})$  and  $\Gamma(t, \mathbf{x}) = \exp[-\lambda t/\mu\sigma^2]\Gamma_{\text{er}}(\mathbf{x})$ , where, in the intruder's frame

$$\begin{aligned} \frac{\mu\sigma^4}{2} \Delta \Phi_{\text{er}} - \mu\sigma^2 \mathbf{v} \cdot \vec{\nabla} \Phi_{\text{er}} + [U_0(\mathbf{x}) + gm_{\text{er}}]\Phi_{\text{er}} &= -\lambda \Phi_{\text{er}} \\ \frac{\mu\sigma^4}{2} \Delta \Gamma_{\text{er}} + \mu\sigma^2 \mathbf{v} \cdot \vec{\nabla} \Gamma_{\text{er}} + [U_0(\mathbf{x}) + gm_{\text{er}}]\Gamma_{\text{er}} &= -\lambda \Gamma_{\text{er}} \end{aligned} \quad (5)$$

(with  $m_{\text{er}} = \Phi_{\text{er}}\Gamma_{\text{er}}$  independent of time). Far from the intruder  $U_0(\mathbf{x}) = 0$ ,  $m \simeq m_0$  and pedestrians have constant velocity  $-\mathbf{v}$  in the intruder's frame. This imposes the asymptotic solutions  $\Phi_{\text{er}}(\mathbf{x}) = \Gamma_{\text{er}}(\mathbf{x}) = \sqrt{m_0}$ , from which  $\lambda = -gm_0$ .

#### IV. RESULTS

The stationary Eqs. (5) have two remarkable features: (i) They give direct access to the permanent regime, and are straightforward to implement numerically since time dependence has disappeared (results with reasonable resolution can be obtained in a few minutes on a mid-range laptop). (ii) As in Ref. [61], rescaling Eqs. (5) shows that solutions are entirely specified by only two dimensionless parameters.

Indeed, the intruder is characterized by its radius  $R$  and its velocity  $v$ . Similarly, pedestrians are characterized by a length scale  $\xi = \sqrt{|\mu\sigma^4/2gm_0|}$ , the distance over which the crowd density tends to recover its bulk value from a perturbation, aka *healing length*, and a velocity scale  $c_s = \sqrt{|gm_0/2\mu|}$ , the typical speed at which pedestrians tend to move.<sup>1</sup> Up to a scaling factor, solutions of Eqs. (5) can be expressed as a function of the two ratios  $\xi/R$  and  $c_s/v$  instead of depending on the full set of parameters  $(R, v, \mu, \sigma, m_0, g)$ , which facilitates the exploration of the parameter space, makes modeling more robust, and highlights the uttermost importance of anticipation. It should be noted that in MFG the individual anticipation time, usually defined explicitly in classical agent-based models, is encoded in the choice of  $\xi$  and  $c_s$  but is not readily available as a function of the two. In fact, MFG leads to a strategy of motion where the anticipation time is optimal, without prescribing it.

Figure 2 presents typical density and velocity fields simulated in the permanent regime for each quadrant of the reduced

<sup>1</sup>Note that  $\mu\xi c_s = \mu\sigma^2$  has the dimension of an action and plays the role of  $\hbar$  in the original nonlinear Schrödinger equation.

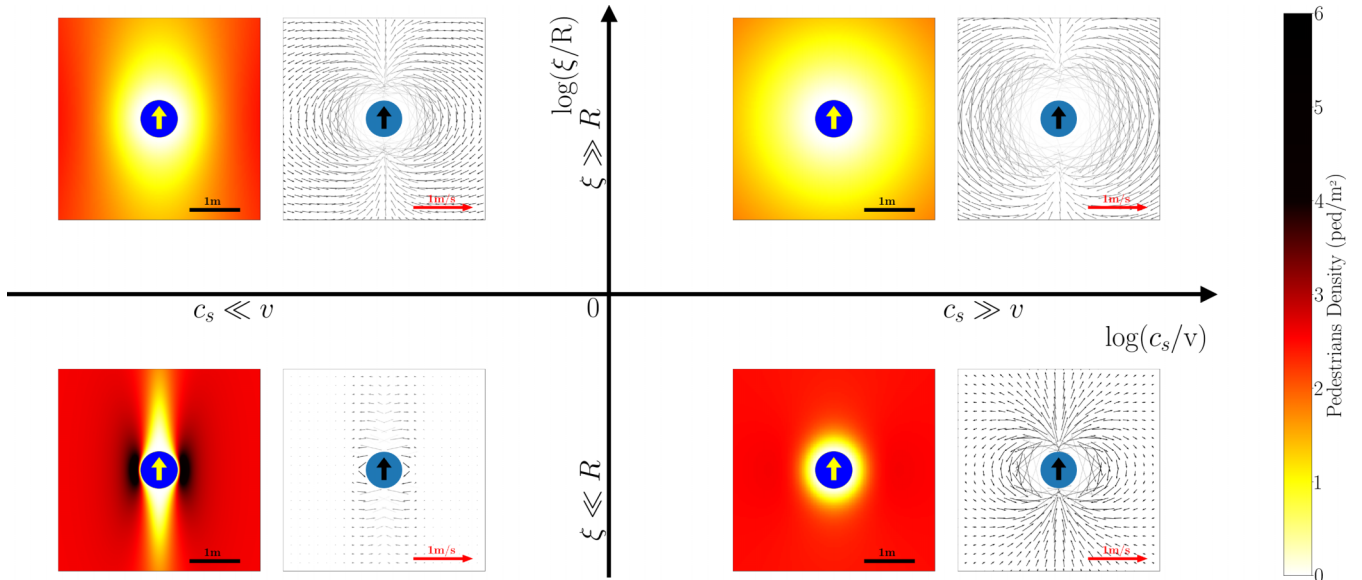


FIG. 2. Typical density and velocity fields induced by the crossing intruder in the permanent regime, as predicted by the MFG model in different regions of the parameter space. Parameters taken in the small  $c_s/v$  and small  $\xi/R$  quadrant display good visual agreement with the experimental data.

parameter space. Intuitively, one understands that  $c_s$  governs the cost of motion for the agents while  $\xi$  gives the extent of the perturbation caused by the presence of the intruder. The main difference between large and small  $c_s/v$  is the change in rotational symmetry, which reflects a fundamental change in strategy. For large values of  $c_s/v$  pedestrians do not mind moving, and they rather try to avoid congested areas for as long as possible, thus creating circulation around the intruder, as shown in the velocity plots. On the other hand, for small values of  $c_s/v$ , moving fast costs more; therefore, to avoid the intruder, pedestrians have to move earlier, and accept to temporarily sidestep into a more crowded area, thereby stretching the density along the vertical direction.

Experimental observations [15] are best reproduced for small  $c_s/v$  and small  $\xi/R$  ( $c_s = 0.11$  and  $\xi = 0.15$ ), as shown in the third column of Fig. 1. Considering the minimalism of our MFG model, the obtained agreement is especially satisfying. In particular, it demonstrates that even basic MFG models can naturally capture prominent features of the response of static crowds which may be out of reach of more short-sighted pedestrian dynamics models.

### V. ALTERNATIVE CONFIGURATION: BOARDING OF A TRAIN

Although our model reproduces remarkably well the experiments of Ref. [15] in view of its minimalism, we realize that a single test might not be sufficient to justify our claim that MFG theory is a good candidate for modeling pedestrian dynamics. We argue that MFGs are also applicable to a broader array of crowd-related problems at the operational level, beyond crossing scenarios. In this section, we illustrate this assertion by exploring the daily-life situation of people waiting to board a coach in an underground station. This is a common configuration at the frontier between the operational and tactical level, which should give a strong edge to MFG

over alternative models, owing to the important role played by anticipation.

This situation can be readily simulated by suitably modifying the external potential  $U_0(\mathbf{x})$  and the geometry of the system, as shown in Fig. 3;  $U_0(\mathbf{x})$  here is a boxlike infinite potential representing the walls of the coach (black bands). On top of that, we introduced a terminal cost  $c_T(\mathbf{x})$  [21,59] that is lower aboard the metro than on the platform,

$$c_T(\mathbf{x}) = c_{\text{platform}} + [c_{\text{coach}} - c_{\text{platform}}]\Theta(x_{\text{wall}} - x), \quad (6)$$

where  $c_{\text{coach}} < c_{\text{platform}}$ ,  $\Theta$  is the Heaviside function and  $x_{\text{wall}}$  is the  $x$  coordinate (horizontal) where the walls of the coach start. This terminal cost  $c_T(\mathbf{x})$  does not modify the MFG equation (3) but serves as terminal condition for the value function  $u(\mathbf{x}, t = T) = c_T(\mathbf{x})$  (and accordingly for  $\Phi$ ). We then numerically solve the nonlinear Schrödinger type system using the algorithm described succinctly in Sec. III and in more detail in Appendix C. Results of our simulations can be seen in Movie S4 [27], of which Fig. 3 (right) is a snapshot.

There are sadly no experimental evidence to support this at the moment, but we manage to reproduce the boarding process in a qualitatively realistic way, despite the simplicity of our model. We even naturally capture the decision made by some agents to stay on the platform rather than board the overcrowded metro. We believe this last point to be particularly interesting since this passive behavior emerges naturally from our (anticipatory) game theoretical model, which would be more difficult to implement in traditional approaches of crowd dynamics.

### VI. DISCUSSION

To conclude, our results have been obtained with a simple, generic MFG model which depends linearly on density via  $gm(t, \mathbf{x})$ . The NLS representation provides important insight, efficient numerical schemes, and powerful analytical tools.

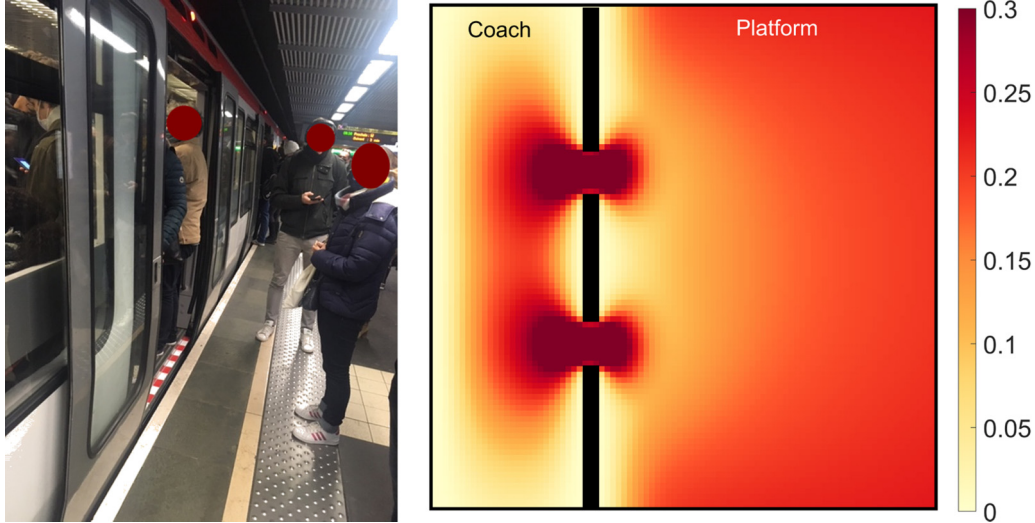


FIG. 3. Boarding a crowded metro coach at rush hour. Left: Morning rush hour of November 18, 2021, on the platform of Metro A in Lyon, France. The doors are about to close and the gap between boarding passengers and those who preferred to wait for the next metro is clearly visible. Right: Snapshot from a MFG simulation at  $t = 0.9T$ . Players start uniformly distributed on the platform and would like to get on the coach before the doors close, at  $t = T$ . Just before that moment, the players closest to the doors choose to rush toward the coach and cram themselves in it despite the high density. Others prefer to stay on the platform (see Movie S4 [27] for the whole process). Simulations have been performed in a box of dimensions  $15 \times 15$  over a time  $T = 10$ , with an initial density on the platform  $m_0 = 0.2$ . Parameters are chosen to have healing length  $\xi = 1.1$ , and speed of sound  $c_s = 0.45$ , while  $c_{\text{coach}} = 0$  and  $c_{\text{platform}} = 6.21$ .

Most notably, it draws a bridge between pedestrian dynamics and optics, fluid dynamics, or Bose-Einstein condensation. Naturally our minimal model can be refined: the MFG formalism is flexible enough to incorporate further elements and make it truer to life, including time-discounting effects [62,63] and congestion [45,64,65]. Higher quantitative accuracy will be within reach of these more sophisticated approaches, possibly at the expense of less transparent outcomes. For sure, MFG will struggle to capture a variety of problems of crowd dynamics at the operational level, notably those for which the granularity of the crowd is central. However, the afore-studied experiments strikingly illustrate that *even the simplest* of MFG model is able to capture qualitative features that generally elude existing agent-based models, even if they include short-time anticipation.

We also believe MFG can apply in various other configurations. In particular, we show in Sec. V an MFG simulation of train-boarding at peak hours that qualitatively reproduces some nontrivial features associated with this situation (Movie S4) [27]. All this bolsters the claim that *optimization* and *anticipation* stand among the essential ingredients for the description of crowd dynamics at the *operational* level, and justifies to claim entry for MFG-based approaches into the toolkit of practitioners of the field.

**ACKNOWLEDGMENTS**

We acknowledge financial support for the internship of Theophile Bonnet by the Investissements d’Avenir of LabEx PALM (ANR-10-LABX-0039-PALM), as part of the PERCEFOULE project, and funding from the Hubert Curien Partnership France-Malaysia Hibiscus (PHC-Hibiscus) Program No. 45687WJ [203.PKOMP.6782005].

**APPENDIX A: GRANULAR SIMULATIONS**

Appendix A provides details on the numerical method used to produce the granular matter simulation, displayed in the first column of Fig. 1 of the main text (also see Movie S1 [27]). The numerical method is adapted from Ref. [66].

To simulate the displacement of an intruder in a two-dimensional granular medium, we resort to molecular dynamics. The diameter of the grains is  $d = 0.37$  m and they all have the same mass. All interactions between two grains  $i$  and  $j$  in the simulation are modeled with a dissipative Hertz law of the form  $F_{ij} = k\zeta^{3/2} - \lambda \frac{d\zeta}{dt}$ , where  $\zeta$  is the interpenetration of the grains,  $k$  is the stiffness of the contact, and  $\lambda$  is a damping coefficient. The stiffness  $k$  is related to the Young’s modulus  $E = 1$  GPa of the grains by  $k = E\sqrt{d/2}$ . The coefficient of viscous damping  $\lambda$  simulates a restitution coefficient  $e = 0.5$ . One can notice that the grains are frictionless. The time step is small enough to ensure numerical convergence. The details of these calculations were reported in Ref. [66]. The diameter of the intruder is  $D = 2d = 0.74$  m and its mechanical properties are identical to those of the grains. The tank containing the granular material is of length  $L_x = 25d$  in the  $x$  direction and  $L_y = 200d$  in the  $y$  direction.

To prepare the initial state, the intruder is initially fixed in the tank. The  $y$  position of the intruder in the  $y$  direction corresponds to the vertical distance from the bottom wall of the tank to the center of the intruder such that  $y = 2.5D$  is the initial vertical position of the intruder. The  $x$  position of the intruder in the  $x$  direction corresponds to the equal distance from the left wall and right wall of the tank to the center of the intruder such that  $x = L_x/2$  is the initial horizontal position of the intruder. Once the intruder is placed, we fill the remaining space by randomly drawing  $x$  and  $y$  positions for each grain.

The number of grains to insert depends on the chosen objective density. We ensure that there is no spatial overlap between the grains. Once the initial configuration has been prepared, we move the intruder at constant velocity  $v = 0.6 \text{ m}\cdot\text{s}^{-1}$  along the  $y$  direction. The intruder runs a distance equivalent almost to  $80D$  in the  $y$  direction to avoid getting too close to the top wall of the tank. The displacement of the intruder in this granular material naturally leaves a wake behind it since there is no pressure scale that comes to fill it up [26,67,68]. To create a process that fills this wake, we introduce a small Gaussian noise in the displacement of the grains during the simulation. This noise acts as diffusion for the displacement which will then have the possibility of filling the wake.

The run of the intruder through the granular medium allows us to get the positions of the grains over time. Considering these data after passing through the spatial transient regime (of the order of one  $D$ ), we reach a stationary regime on average for the grain flow around the intruder. For each simulation, we can calculate the density field and the velocity field around the intruder. To smooth the results, they have been averaged over 10 runs of intruder displacement.

## APPENDIX B: AGENT-BASED MODEL FOR PEDESTRIAN DYNAMICS BASED ON AN ANTICIPATED TIME TO COLLISION

Appendix B provides details on the numerical methods used to produce the agent-based simulations, displayed in the second column of Fig. 1 of the main text (also see Movie S2 [27]).

### 1. Principle

The social force model, initially propounded by Helbing and Molnar [7], arguably remains the continuous model that is most widely used commercially to simulate pedestrian dynamics. In this model, agents essentially obey Newtonian dynamics, with a sum of binary pseudoforces (social forces) mimicking their attractive and repulsive interactions with neighboring agents, which are mostly based on their relative positions.

However, it has been shown that substituting these positional variables with a time-to-collision (TTC) variable, reflecting the time at which each agent expects the most imminent collision with other agents, better renders the spatial organization of pedestrians in diverse empirical settings [9]. The agent-based model used in the main text to represent a crowd of agents displaying some degree of anticipation is based on the same approach, but incorporates a number of changes aimed at correcting some issues as identified in Karamouzas *et al.*'s seminal paper [9].

First, to enhance numerical stability, instead of solving a Newtonian equation with a TTC-based force, we opt for a numerical scheme in which the velocities selected at each time step result from the minimization of a total energy (including the TTC contribution), following Ref. [12]. Nonetheless, contrary to Ref. [12], each agent minimizes their own energy, rather than solving for the set of agents' velocities that minimizes the global energy of the assembly; these individual choices better reflect the decisional process at play in a

crowd of autonomous agents (and not robots), in line with the concept of utility used in economics rather than the global energy used in physics [69]. Besides, only the most imminent collision is taken into account to compute the TTC energy. Finally, to avoid grazing trajectories and smooth the agents' response [70], each agent is modeled as a disk whose radius is uncertain, i.e., estimated between  $R$  and  $(1 + \epsilon)R$ . In addition to avoiding discontinuities in the collision avoidance response, this uncertainty accounts for the existence of an immaterial private sphere around each agent, which others are reluctant to cross.

All in all, the total energy  $E[\mathbf{v}'_p]$  minimized by each agent with respect to their velocity  $\mathbf{v}'_p$  comprises the following contributions:

(1) A driving term  $E^{\text{target}} = \text{FF}(\mathbf{r} + \tau_\phi \mathbf{v}'_p)$  with a static floor field FF giving the shortest-path distance to a target or a set of targets, computed with the Dijkstra algorithm. Here,  $\tau_\phi$  is a reaction time and  $\mathbf{r} + \tau_\phi \mathbf{v}'_p$  is the position at which the agent expects to be after this reaction time, should they choose velocity  $\mathbf{v}'_p$ .

(2) A term constraining the agent's speed,  $E^{\text{speed}} = \alpha v'_p (\mathbf{v}'_p - \mathbf{v}_p^{\text{pref}})^2$ , where  $v'_p = \|\mathbf{v}'_p\|$ . Note that  $v'_p = 0$  is a minimum of this term, which means that not moving is a suitable option for static agents, as it should be.

(3) A term penalizing sudden changes in velocity (direction), compared to the current velocity  $\mathbf{v}_p^t$ ,  $E^{\text{inertia}} = \beta |\mathbf{v}'_p - \mathbf{v}_p^t|^2 \Delta t^{-2}$ .

(4) An interpedestrian repulsion term,  $E^{\text{core-repulsion}} = \eta (\frac{1}{d} - \frac{1}{d^*})$ , with  $d$  the actual distance between pedestrians and  $d^*$  a threshold distance beyond which this term is no longer zero. Here,  $\epsilon$  takes into account the uncertainty that each pedestrian has when estimating the radii of their neighbors.

(5) The TTC energy  $E_i^{\text{TTC}} = \max_j E^{\text{TTC}}(\tau_{ij})$ , where  $\tau_{ij}$  is the anticipated TTC between agent  $i$  and agent  $j$  under the assumption that the current velocities are maintained and  $E^{\text{TTC}}$  is the TTC energy expression given by Ref. [9], which we characterize with the parameter  $\gamma$ . This is actually the most important term in our model. Should it be turned off, particles would stop anticipating the upcoming intrusion.

The minimization over  $\mathbf{v}_p$  is performed with the Nelder-Mead algorithm for each agent and the updating scheme is made via

$$\begin{aligned} \mathbf{v}_p^{t+1} &= \underset{\mathbf{v}'_p}{\text{argmin}} (E[\mathbf{v}'_p]), \\ \mathbf{x}^{t+1} &= \mathbf{x}^t + \mathbf{v}_p^{t+1} \cdot \Delta t, \end{aligned}$$

with a time step  $\Delta t = 0.1 \text{ s}$  (lower values of  $\Delta t$  were also used to test the convergence of the implemented framework with no significant changes).

### 2. Simulation layout

To simulate the crossing of a static crowd by an intruder, the model is specified as follows:

The floor-field energy  $E^{\text{target}}$  is specific to each agent, with a target that matches their initial position. The interaction with the intruder (and other particles) will make them move away from this position, but they will strive to come back to it once it has passed. The speed term in the energy is computed

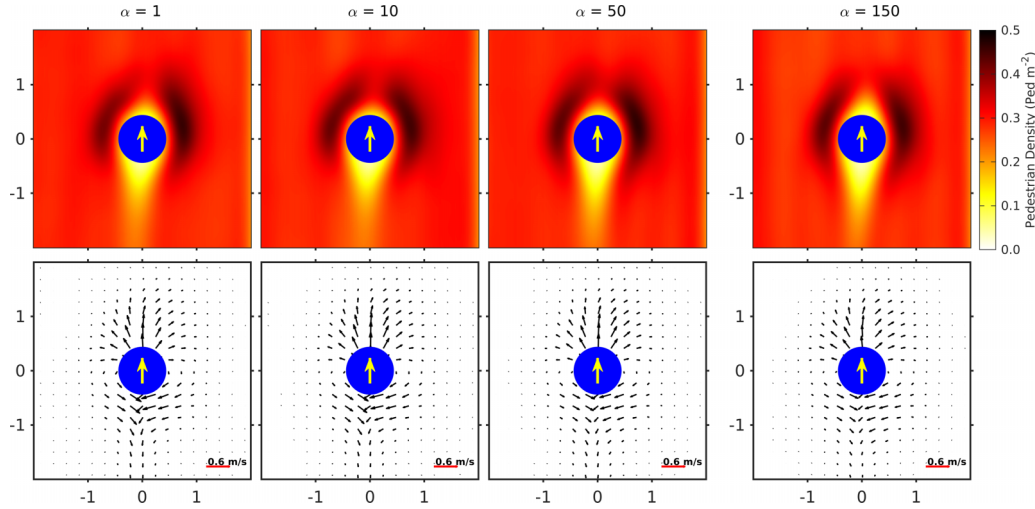


FIG. 4. Variation of the agent speed term for the TTC model, while keeping the other parameters equal to those of the picture displayed in the letter.

with a preferential speed  $v_p^{pref}$  coinciding with experimental measurements for the avoidance response.

Regarding the geometry, an intruder of diameter  $D = 0.74$  m has to cross a region of 20 m length  $\times$  4 m width along its median part. The intruder moves uniformly and linearly along the  $y$ -axis at a prescribed speed  $v = 0.5 \text{ m} \times \text{s}^{-1}$ . Inside this zone, 200 particles (thus obtaining a global density of  $2.5 \text{ ped/m}^2$ ) of diameter  $d = D/2$  are randomly distributed.

The results presented in the main text correspond to moments when the intruder is at least 3 m from the boundaries (entrance and exit of the corridor). This was done in an attempt to minimize boundary effects in the measurements and achieve an approximately stationary state.

For the sake of completeness, we include here an exhaustive exploration of parameter space determined by the values of  $\alpha$ ,  $\beta$ , and  $\gamma$ .

Indeed, Figs. 4–6 show the density and velocity plots for the TTC model for four different choices of these parameters. For each figure, the rightmost columns shows the results for

the values used in the paper, whereas the other three columns show the variation of one of the three parameters, leaving the other two untouched. By observing these figure, we can conclude that the fundamental parameter of the TTC model is indeed the TTC amplitude term  $\gamma$ , indeed the only one capable to produce significant variations of the solution. The other two parameters, while introducing some changes in the velocity plots, do not have a real impact on the main features we look for, such as the horizontal displacement and the lateral accumulation of the agents.

APPENDIX C: MEAN-FIELD GAME SIMULATIONS

This third and last section describes the numerical schemes used to produce MFG simulations. Results of a time-independent simulation are displayed in the third column of the Fig. 1 of the main text, whereas time-dependent ones are used to simulate metro-boarding. Naturally, we expect

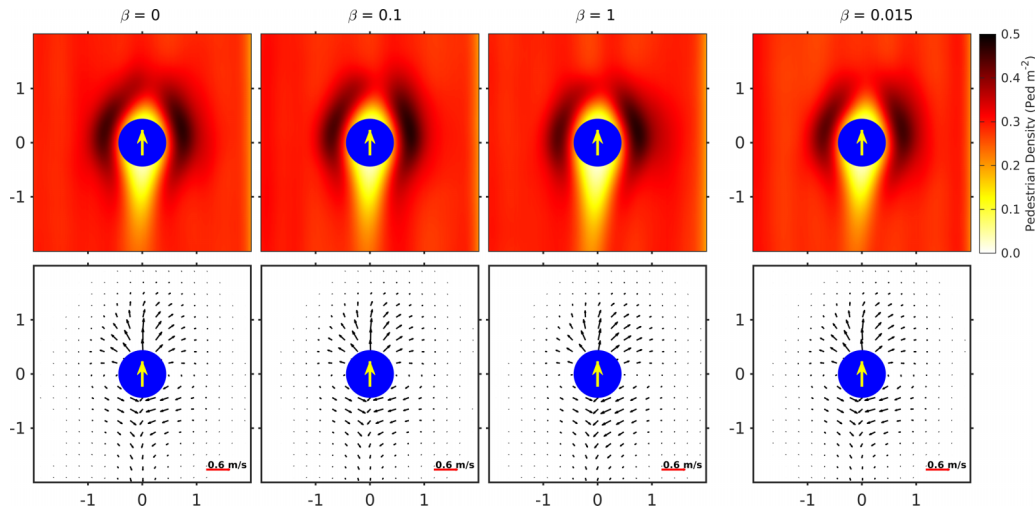


FIG. 5. Variation of the inertial term for the TTC model, while keeping the other parameters equal to those of the picture displayed in the letter.

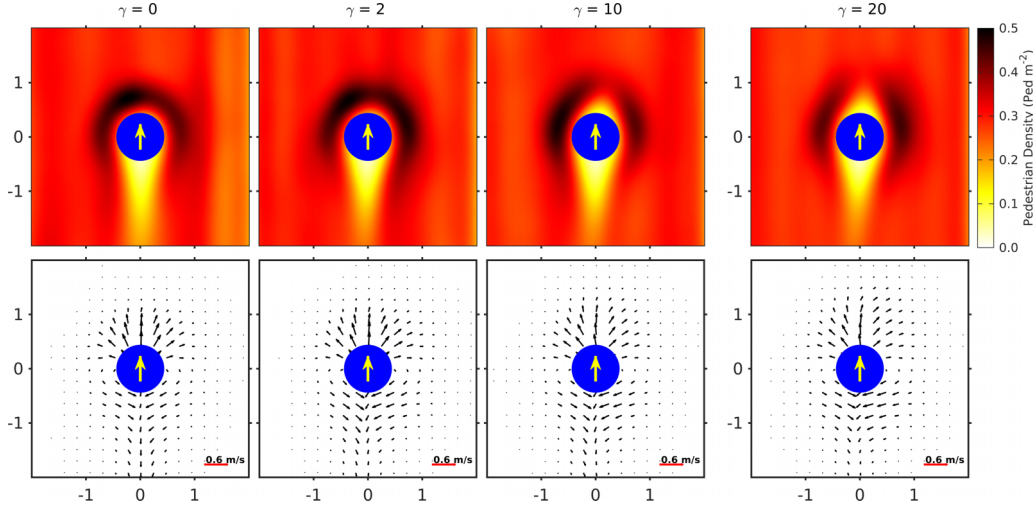


FIG. 6. Variation of the TTC amplitude term for the TTC model, while keeping the other parameters equal to those of the picture displayed in the paper.

both schemes to be consistent in the appropriate regime as evidenced by Movie S3 [27].

### 1. Time-independent MFG

The equation we want to solve numerically is the first of system (5), which we recall,

$$\frac{\mu\sigma^4}{2}\Delta\Phi - \mu\sigma^2 v \partial_y \Phi + (gm + U_0(\vec{x}))\Phi = -\lambda\Phi, \quad (\text{C1})$$

where  $\lambda = -gm_0$ . We want to solve the equation in a box of side  $L$ . We define the matrices  $\Phi \in \mathbb{R}^{N,N}$  and  $\Gamma \in \mathbb{R}^{N,N}$  that we have to evaluate on a grid of  $N \times N$  points corresponding

to the  $(x, y)$  coordinates in Euclidean space. To do this, we first write the discrete form of Eq. (C1),

$$\begin{aligned} & \frac{\mu\sigma^4}{2dx^2}(\Phi_{i-1,j} + \Phi_{i+1,j} + \Phi_{i,j-1} + \Phi_{i,j+1} - 4\Phi_{i,j}) \\ & - \mu\sigma^2 v \frac{\Phi_{i,j+1} - \Phi_{i,j-1}}{2dy} + (gm_{i,j} + V_0V_{i,j})\Phi_{i,j} \\ & = -\lambda\Phi_{i,j}, \end{aligned}$$

where we choose  $dx = dy$ . Then we make the term  $\Phi_{i,j}$  explicit and obtain

$$\Phi_{i,j}^{k+1} = \frac{\frac{\mu\sigma^4}{2}(\Phi_{i-1,j}^k + \Phi_{i+1,j}^k + \Phi_{i,j-1}^k + \Phi_{i,j+1}^k) - \frac{\mu\sigma^2}{2}vdx(\Phi_{i,j+1}^k - \Phi_{i,j-1}^k)}{2\mu\sigma^4 - \lambda dx^2 - (gm_{i,j} + V_0V_{i,j})dx^2}.$$

This is the recursive rule that updates  $\Phi_{i,j}$  until convergence. For a generic geometry, the same rule with an opposite sign of  $v$  would be used to find  $\Gamma_{i,j}$ . Here we take advantage of the symmetry  $\Phi \rightarrow \Gamma$  and  $(x, y) \rightarrow (x, -y)$  to directly obtain  $\Gamma$ . Starting from an initial guess for  $\Phi$ ,  $\Gamma$ , and  $m$ , we fix boundary conditions given by the asymptotic solution  $\Phi_{er}(\mathbf{x}) = \sqrt{m_0}$ , then iterate the formula to find  $\Phi$  and  $\Gamma$ , and, recalling that  $\Phi\Gamma = m$ , also the density. We repeat this operation until convergence of  $m$ .

### 2. Time-dependent MFG

Time-dependent simulations were realized using a C++ algorithm, using the Schrödinger representation of MFG equations to lean on the symmetry between the fields  $\Phi$  and  $\Gamma$  and on well-proven numerical methods such as the Crank-Nicolson [71,72] implicit scheme which provides added stability compared to Euler method. Details of the discretization, along with a stability analysis of the method, can be found in Appendix A of Ref. [73].

The forward-backward conditions, along with the nonlinear coupling between the fields, make direct resolution of

MFG equations difficult. A simple, though not perfectly controlled, way to bypass those difficulties is to solve the system iteratively:

(1) Assume a plausible form of the density  $m^0$  (e.g., a constant equal to the average density).

(2) Compute, using the Crank-Nicolson scheme, a first solution  $\Phi^1$  of the backward equation

$$-\mu\sigma^2 \partial_t \Phi^1 = \frac{\mu\sigma^4}{2} \Delta \Phi^1 + (U_0 + gm^0)\Phi^1, \quad (\text{C2})$$

with given terminal condition  $\Phi(T, \mathbf{x})$ .

(3) Compute  $\Gamma^1$ , solution of the forward equation

$$\mu\sigma^2 \partial_t \Gamma^1 = \frac{\mu\sigma^4}{2} \Delta \Gamma^1 + (U_0 + gm^0)\Gamma^1, \quad (\text{C3})$$

with initial condition  $m^0(\mathbf{x}, t=0)/\Phi^1(\mathbf{x}, t=0)$ .

(4) Update the initial guess  $m^0 \rightarrow m^1 = \Phi^1\Gamma^1$  and repeat the process until  $m^n$  is sufficiently close to  $m^{n-1}$ . In practice, we check for

$$\max_{\mathbf{x}, t} |m^n(\mathbf{x}, t) - m^{n-1}(\mathbf{x}, t)| < \epsilon. \quad (\text{C4})$$

(We will use  $\epsilon = 0.001$ , which we expect to be sufficiently small given the average density  $m_0 = 2.5$ , in accordance with the experiments of Ref. [15].)

This method is easy to implement and fairly efficient, but in some particular circumstances convergence may not occur. This may be alleviated by updating the guess differently,

$$m^{i+1} = \alpha m^i + (1 - \alpha) \Phi^{i+1} \Gamma^{i+1}, \quad (\text{C5})$$

$\alpha$  being a suitable number between 0 and 1.

The complete dynamics of the time-dependent MFG can be found in Movie S3 [27]. All MFG simulations are

realized with parameters  $\xi = 0.15$  and  $c_s = 0.11$ . In the time-dependent simulations, the intruder (of diameter  $D = 0.74$  and velocity  $v = 0.5$ ) crosses vertically a static crowd in a box of dimensions  $6 \times 11$  (with periodic boundary conditions) over a time  $T = 27.5$  long enough to reach the ergodic state. The time-independent simulation is performed in a box of side  $L = 40$ , large enough so differences between the boundary conditions of the two approaches are negligible. As proof of the soundness of both approaches, comparison between the time-dependent simulation at  $t \simeq T/2$  and the time-independent results shows excellent agreement.

- 
- [1] D. Helbing, A. Johansson, and H. Z. Al-Abideen, Dynamics of crowd disasters: An empirical study, *Phys. Rev. E* **75**, 046109 (2007).
- [2] S. P. Hoogendoorn and P. H. Bovy, Pedestrian route-choice and activity scheduling theory and models, *Transp. Res. Part B: Methodol.* **38**, 169 (2004).
- [3] Y.-Q. Jiang, W. Zhang, and S.-G. Zhou, Comparison study of the reactive and predictive dynamic models for pedestrian flow, *Phys. A: Stat. Mech. Appl.* **441**, 51 (2016).
- [4] B. L. Mesmer and C. L. Bloebaum, Incorporation of decision, game, and Bayesian game theory in an emergency evacuation exit decision model, *Fire Saf. J.* **67**, 121 (2014).
- [5] A. Best, S. Narang, S. Curtis, and D. Manocha, Densesense: Interactive crowd simulation using density-dependent filters, in *Proceedings of the ACM SIGGRAPH/Eurographics Symposium on Computer Animation* (ACM Press, New York, 2014), pp. 97–102.
- [6] A. van Goethem, N. Jaklin, A. C. IV, and R. Geraerts, On streams and incentives—a synthesis of individual and collective crowd motion, in *Proceedings of the 28th International Conference on Computer Animation and Social Agents (CASA)* (2015).
- [7] D. Helbing and P. Molnar, Social force model for pedestrian dynamics, *Phys. Rev. E* **51**, 4282 (1995).
- [8] F. Zanlungo, T. Ikeda, and T. Kanda, Social force model with explicit collision prediction, *Europhys. Lett.* **93**, 68005 (2011).
- [9] I. Karamouzas, B. Skinner, and S. J. Guy, Universal Power Law Governing Pedestrian Interactions, *Phys. Rev. Lett.* **113**, 238701 (2014).
- [10] J. van den Berg, M. C. Lin, and D. Manocha, Reciprocal velocity obstacles for real-time multi-agent navigation, in *Proceedings of the 2008 IEEE International Conference on Robotics and Automation* (IEEE, Washington, 2008), pp. 1928–1935.
- [11] S. Paris, J. Pettré, and S. Donikian, Pedestrian reactive navigation for crowd simulation: A predictive approach, in *Computer Graphics Forum* (Wiley Online Library, London, 2007), Vol. 26, pp. 665–674.
- [12] I. Karamouzas, N. Sohre, R. Narain, and S. J. Guy, Implicit crowds: Optimization integrator for robust crowd simulation, *ACM Trans. Graph.* **36**, 1 (2017).
- [13] M. Moussaïd, D. Helbing, and G. Theraulaz, How simple rules determine pedestrian behavior and crowd disasters, *Proc. Natl. Acad. Sci. USA* **108**, 6884 (2011).
- [14] J. Bruneau and J. Pettré, EACS: Effective avoidance combination strategy, *Comput. Graph. Forum* **36**, 108 (2017).
- [15] A. Nicolas, M. Kuperman, S. Ibañez, S. Bouzat, and C. Appert-Rolland, Mechanical response of dense pedestrian crowds to the crossing of intruders, *Sci. Rep.* **9**, 105 (2019).
- [16] B. Kleinmeier, G. Köster, and J. Drury, Agent-based simulation of collective cooperation: From experiment to model, *J. R. Soc. Interface* **17**, 20200396 (2020).
- [17] J.-M. Lasry and P.-L. Lions, Mean field games I. The stationary case? *C. R. Math.* **343**, 619 (2006).
- [18] J.-M. Lasry and P.-L. Lions, Mean field games II. Finite time horizon and optimal control? *C. R. Math.* **343**, 679 (2006).
- [19] M. Huang, R. P. Malhamé, and P. E. Caines, Large population stochastic dynamic games: Closed-loop McKean-Vlasov systems and the Nash certainty equivalence principle, *Commun. Inform. Syst.* **6**, 221 (2006).
- [20] O. Guéant, Mean field games equations with quadratic Hamiltonian: A specific approach, *Math. Models Methods Appl. Sci.* **22**, 1250022 (2012).
- [21] D. Ullmo, I. Swiecicki, and T. Gobron, Quadratic mean field games, *Phys. Rep.* **799**, 1 (2019).
- [22] C. Appert-Rolland, J. Pettré, A.-H. Olivier, W. Warren, A. Duigou-Majumdar, E. Pinsard, and A. Nicolas, Experimental study of collective pedestrian dynamics, *Collect. Dyn.* **5**, A109 (2020).
- [23] <https://twitter.com/AmichaiStein1/status/1140374111258140673>.
- [24] A. Seguin, Y. Bertho, P. Gondret, and J. Crassous, Dense Granular Flow Around a Penetrating Object: Experiment and Hydrodynamic Model, *Phys. Rev. Lett.* **107**, 048001 (2011).
- [25] A. Seguin, Y. Bertho, F. Martinez, J. Crassous, and P. Gondret, Experimental velocity fields and forces for a cylinder penetrating into a granular medium, *Phys. Rev. E* **87**, 012201 (2013).
- [26] A. Seguin, A. Lefebvre-Lepot, S. Faure, and P. Gondret, Clustering and flow around a sphere moving into a grain cloud, *Eur. Phys. J. E* **39**, 63 (2016).
- [27] See the associated movies deposited on the Open Science Foundation website at [https://osf.io/hytd/?view\\_only=a5c81b95c08e4604b8d3845c16e22b57](https://osf.io/hytd/?view_only=a5c81b95c08e4604b8d3845c16e22b57).
- [28] M. Danny Raj and V. Kumaran, Moving efficiently through a crowd: A nature-inspired traffic rule, *Phys. Rev. E* **104**, 054609 (2021).
- [29] S. Heliövaara, H. Ehtamo, D. Helbing, and T. Korhonen, Patient and impatient pedestrians in a spatial game for egress congestion, *Phys. Rev. E* **87**, 012802 (2013).

- [30] S. Bouzat and M. N. Kuperman, Game theory in models of pedestrian room evacuation, *Phys. Rev. E* **89**, 032806 (2014).
- [31] A. Lachapelle, J. Salomon, and G. Turinici, A monotonic algorithm for a mean field games model in economics, *Les Cahiers de la Chaire (Finance & Développement Durable)* 16, (2009).
- [32] P. Cardaliaguet and C.-A. Lehalle, Mean field game of controls and an application to trade crowding, *Math. Finan. Econ.* **12**, 335 (2018).
- [33] R. Carmona, F. Delarue, and A. Lachapelle, Control of McKean-Vlasov dynamics versus mean field games, *Math. Finan. Econ.* **7**, 131 (2013).
- [34] Y. Achdou, P.-N. Giraud, J.-M. Lasry, and P.-L. Lions, A long-term mathematical model for mining industries, *Appl. Math. Optim.* **74**, 579 (2016).
- [35] O. Guéant, J.-M. Lasry, and P.-L. Lions, Mean field games and applications, in *Paris-Princeton Lectures on Mathematical Finance 2010* (Springer, Berlin, Heidelberg, 2011).
- [36] Y. Achdou, F. J. Buera, J.-M. Lasry, P.-L. Lions, and B. Moll, Partial differential equation models in macroeconomics, *Philos. Trans. R. Soc. A.* **372**, 20130397 (2014).
- [37] L. Laguzet and G. Turinici, Individual vaccination as Nash equilibrium in a SIR model with application to the 2009-2010 influenza a (H1N1) epidemic in france, *Bull. Math. Biol.* **77**, 1955 (2015).
- [38] R. Djidjou-Demasse, Y. Michalakis, M. Choisy, M. T. Sofonea, and S. Alizon, Optimal COVID-19 epidemic control until vaccine deployment, medRxiv 2020.04.02.20049189, doi:<https://doi.org/10.1101/2020.04.02.20049189>.
- [39] R. Elie, E. Hubert, and G. Turinici, Contact rate epidemic control of COVID-19: An equilibrium view, *Math. Modell. Nat. Phenom.* **15**, 35 (2020).
- [40] A. Lachapelle and M.-T. Wolfram, On a mean field game approach modeling congestion and aversion in pedestrian crowds, *Transp. Res. Part B: Methodol.* **45**, 1572 (2011).
- [41] Y. Achdou, M. Bardi, and M. Cirant, Mean field games models of segregation, *Math. Models Methods Appl. Sci.* **27**, 75 (2017).
- [42] A. C. Kizilkale and R. P. Malhamé, Load shaping via grid wide coordination of heating-cooling electric loads: A mean field games based approach, <https://www.gerad.ca/fr/papers/G-2015-68>.
- [43] A. C. Kizilkale, R. Salhab, and R. P. Malhamé, An integral control formulation of mean field game based large scale coordination of loads in smart grids, *Automatica* **100**, 312 (2019).
- [44] F. Mériaux, V. S. Varma, and S. Lasaulce, Mean field energy games in wireless networks, in *Proceedings of the 2012 Conference Record of the Forty Sixth Asilomar Conference on Signals, Systems and Computers* (IEEE, New York, 2012).
- [45] O. Guéant, Existence and uniqueness result for mean field games with congestion effect on graphs, *Appl. Math. Optim.* **72**, 291 (2015).
- [46] Y.-Q. Jiang, R.-Y. Guo, F.-B. Tian, and S.-G. Zhou, Macroscopic modeling of pedestrian flow based on a second-order predictive dynamic model, *Appl. Math. Modell.* **40**, 9806 (2016).
- [47] B. Djehiche, A. Tcheukam, and H. Tembine, A mean-field game of evacuation in multilevel building, *IEEE Trans. Autom. Control* **62**, 5154 (2017).
- [48] N. Nasser, A. El Ouadrhiri, M. El Kamili, A. Ali, and M. Anan, Crowd management services in Hajj: A mean-field game theory approach, in *Proceedings of the 2019 IEEE Wireless Communications and Networking Conference (WCNC)* (IEEE, Washington, 2019), pp. 1–7.
- [49] D. M. Kreps, Nash equilibrium, *Game Theory* (Springer, London, 1989), pp. 167–177.
- [50] R. Bellman, Dynamic programming, Rand Corporation research study, Princeton University Press, 1957.
- [51] T. Bonnemain, T. Gobron, and D. Ullmo, Universal behavior in non-stationary mean field games, *Phys. Lett. A* **384**, 126608 (2020).
- [52] D. J. Kaup, Perturbation theory for solitons in optical fibers, *Phys. Rev. A* **42**, 5689 (1990).
- [53] F. Copie, S. Randoux, and P. Suret, The Physics of the one-dimensional nonlinear Schrödinger equation in fiber optics: rogue waves, modulation instability and self-focusing phenomena, *Rev. Phys.* **5**, 100037 (2020).
- [54] L. Pitaevskii and S. Stringari, *Bose-Einstein Condensation and Superfluidity* (Oxford University Press, Oxford, 2016), Vol. 164.
- [55] R. Koch, J. S. Caux, and A. Bastianello, Generalized hydrodynamics of the attractive non-linear Schrödinger equation, *J. Phys. A: Math. Theor.* **55**, 134001 (2022).
- [56] C. Kharif, E. Pelinovsky, and A. Slunyaev, *Rogue Waves in the Ocean*, Advances in Geophysical and Environmental Mechanics and Mathematics (Springer, Berlin, 2008).
- [57] G. A. El, E. G. Khamis, and A. Tovbis, Dam break problem for the focusing nonlinear Schrödinger equation and the generation of rogue waves, *Nonlinearity* **29**, 2798 (2016).
- [58] E. Hopf, The partial differential equation  $u_t + uu_x = \mu xx$ , *Commun. Pure Appl. Math.* **3**, 201 (1950).
- [59] T. Bonnemain, T. Gobron, and D. Ullmo, Schrödinger approach to mean field games with negative coordination, *SciPost Phys.* **9**, 059 (2020).
- [60] P. Cardaliaguet, J. Lasry, P. Lions, and A. Porretta, Long time average of mean field games with a nonlocal coupling, *SIAM J. Control Optim.* **51**, 3558 (2013).
- [61] T. Bonnemain, T. Gobron, and D. Ullmo, Lax connection and conserved quantities of quadratic mean field games, *J. Math. Phys.* **62**, 083302 (2021).
- [62] S. Frederick, G. Loewenstein, and T. O'donoghue, Time discounting and time preference: A critical review, *J. Econ. Lit.* **40**, 351 (2002).
- [63] D. A. Gomes, L. Nurbekyan, and E. Pimentel, *Economic Models and Mean-Field Games Theory* (Publicacoes Matematicas, IMPA, Rio, Brazil, 2015).
- [64] C. Dogbé, Modeling crowd dynamics by the mean-field limit approach, *Math. Comput. Modell.* **52**, 1506 (2010).
- [65] Y. Achdou and A. Porretta, Mean field games with congestion, *Ann. Inst. Henri Poincaré C* **35**, 443 (2018).
- [66] A. Seguin, Y. Bertho, P. Gondret, and J. Crassous, Sphere penetration by impact in a granular medium: A collisional process, *Europhys. Lett.* **88**, 44002 (2009).
- [67] R. Candelier and O. Dauchot, Journey of an intruder through the fluidization and jamming transitions of a dense granular media, *Phys. Rev. E* **81**, 011304 (2010).
- [68] E. Kolb, P. Cixous, N. Gaudouen, and T. Darnige, Rigid intruder inside a two-dimensional dense granular flow: Drag force and cavity formation, *Phys. Rev. E* **87**, 032207 (2013).
- [69] S. Grauwil, E. Bertin, R. Lemoy, and P. Jensen, Competition between collective and individual dynamics, *Proc. Natl. Acad. Sci. USA* **106**, 20622 (2009).

- [70] Z. Forootaninia, I. Karamouzas, and R. Narain, *Robotics: Science and Systems* (Cambridge, Massachusetts, 2017), Vol. 7.
- [71] D. Harder, *The Crank-Nicolson Method and Insulated Boundaries* (University of Waterloo, Ontario, Canada, 2012).
- [72] Y. Y. Choy, W. N. Tan, K. G. Tay, and C. T. Ong, Crank-nicolson implicit method for the nonlinear Schrodinger equation with variable coefficient, *AIP Conf. Proc.* **1605**, 76 (2014).
- [73] T. Bonnemain, Quadratic mean field games with negative coordination, Ph.D. theses, Diss. Université Cergy Pontoise, 2020.